Applied Energy 130 (2014) 139–147

Contents lists available at ScienceDirect

Applied Energy

journal homepage: www.elsevier.com/locate/apenergy

Effects of SOC-dependent electrolyte viscosity on performance of vanadium redox flow batteries

Q. Xu, T.S. Zhao *, C. Zhang

Department of Mechanical and Aerospace Engineering, The Hong Kong University of Science and Technology, Clear Water Bay, Kowloon, Hong Kong SAR, China

HIGHLIGHTS

- The correlations of electrolyte viscosity and SOC are obtained.
- Effect of SOC-dependent electrolyte viscosity is considered in this model.
- This model enables a more realistic simulation of variable distributions.
- It provides accurate estimations of pumping work and system efficiency.

ARTICLE INFO

Article history:
Received 29 March 2014
Received in revised form 15 May 2014
Accepted 16 May 2014
Available online 6 June 2014

Keywords:
Flow battery
Vanadium redox flow battery (VRFB)
Numerical modeling
Electrolyte viscosity
Cell performance

ABSTRACT

The viscosity of the electrolyte in vanadium redox flow batteries (VRFBs) varies during charge and discharge as the concentrations of acid and vanadium ions in the electrolyte continuously change with the state of charge (SOC). In previous VRFB models, however, the electrolyte has been treated as a constant-viscosity solution. In this work, a mass-transport and electrochemical model taking account of the effect of SOC-dependent electrolyte viscosity is developed. The comparison between the present model and the model with the constant-viscosity simplification indicates that the consideration of the SOC-dependent electrolyte viscosity enables (i) a more realistic simulation of the distributions of overpotential and current density in the electrodes, and (ii) more accurate estimations of pumping work and the system efficiency of VRFBs.

1. Introduction

The all-vanadium redox flow battery (VRFB) was initially proposed by NASA in mid-1970s and developed by Skyllas-Kazacos et al. in the 1980s, using the V(II)/V(III) and V(IV)/V(V) redox couples in sulfuric acid solution as the anolyte and catholyte, respectively [1–3]. This type of battery is particularly suitable for large-scale storage of intermittent power generated from solar cells and wind turbines due to its unique features, including independent scaling of energy and power ratings, a long cycle life, quick response, a low cost, and the tolerance to deep discharge without any risk of damage [4–7].

A typical single vanadium redox flow cell consists of two porous carbon electrodes and two circulating electrolyte solutions separated by an ion-exchange membrane. The reactions that occur in the electrodes can be expressed as:

$$\text{at the negative electrode}: \quad V^{3+} + e^- \underset{\text{Discharge}}{\overset{\text{Charge}}{\rightleftarrows}} V^{2+} \tag{1}$$

$$\text{at the positive electrode}: \quad VO^{2+} + H_2O - e^- \underset{\text{Discharge}}{\overset{\text{Charge}}{\rightleftarrows}} VO_2^+ + 2H^+ \tag{2}$$

The energy conversion between electrical energy and chemical potential occurs at the electrodes once the liquid electrolytes flow through the cell. Protons transfer through the membrane, while electrons transfer through an external load to form an electrical circuit during charge or discharge process. As a key component of the battery, the electrolyte needs to be highly concentrated to all the vanadium ions, stable and less viscous, as these properties are closely related to the capacity, power and the parasitic energy loss of the battery [8,9]. The concentration of each vanadium ion with a certain valence in the electrolyte keeps changing during the charge and discharge cycle, while the total vanadium ions concentration is approximately constant in both the positive and negative electrolytes. To describe the relative amount of vanadium ions with different valences, the state of charge (SOC) is defined as:

* Corresponding author. Tel.: +852 2358 8647.
E-mail address: metzhao@ust.hk (T.S. Zhao).

http://dx.doi.org/10.1016/j.apenergy.2014.05.034
0306-2619/

$$\mathrm{SOC} = \left(\frac{c_{V(II)}}{c_{V(total)}}\right)_1 = \left(\frac{c_{V(V)}}{c_{V(total)}}\right)_2 \quad (3)$$

where $c_{V(II)}$ and $c_{V(V)}$ are the molar concentrations of V^{2+}, VO_2^+, $c_{V(total)}$ is the total vanadium ions concentration in a certain electrolyte, and the subscripts 1 and 2 represent the negative and positive electrode, respectively.

Alternatively, SOC can also be defined as:

$$\mathrm{SOC} = \left(1 - \frac{c_{V(III)}}{c_{V(total)}}\right)_1 = \left(1 - \frac{c_{V(IV)}}{c_{V(total)}}\right)_2 \quad (4)$$

where $c_{V(III)}$ and $c_{V(IV)}$ are the molar concentrations of V^{3+} and VO^{2+}.

In addition to vanadium ions at different oxidation states, protons and sulphate ions also appear in the battery. In the normal operation, these spectator ions do not take part in the reactions, but they are essential for maintaining conservation of mass and the charge balance in electrolytes. Taking the charge process as example, when the anolyte and catholyte components change from SOC = 0 to SOC = 1, as shown in Fig. 1, the proton concentration increases by 0.5 M in both the anolyte and catholyte if the secondary ionization of sulfuric acid is ignored.

The viscosity of a solution is related to the components and their respective concentrations [10,11]. For a VRFB, the variation in the electrolyte component concentrations will result in a continuous change in the electrolyte viscosity during the charge and discharge cycle [12–16]. Such a SOC-dependent viscosity is expected to cause different effects, as opposed to those resulting from the constant viscosity assumption [17–23], on the velocity field, the concentration and overpotential distributions, and the battery performance. The objective of this work is to study the effects of SOC-dependent electrolyte viscosity by developing a new model as presented below.

2. Mathematical model

Fig. 2 shows the schematic illustration of a single vanadium redox flow cell, which consists of a Nafion 115 membrane in the middle, two graphite felts as electrodes on two sides of the membrane and two current collectors. Sulfuric acid solution containing vanadium ions is used as the positive and negative electrolytes, which are stored in respective reservoirs and pumped to the porous electrodes of the cell. The geometric parameters of the VRFB are listed in Table 1.

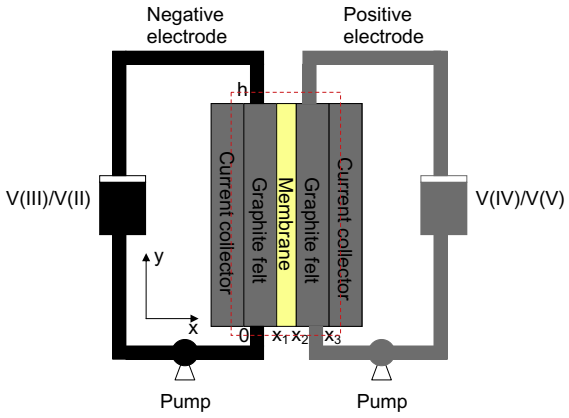

Fig. 2. Schematic of the modeling domain of a VRFB.

2.1. Simplifications and assumptions

We consider a two-dimensional system with the x-axis located in the lower boundary of the battery and the y-axis located at the interface between the negative current collector and graphite felt. Other simplifications and assumptions used in the present work are as follows:

(1) As indicated in Eqs. (3) and (4), in general, SOC varies with time. However, in the case when the reservoir is sufficiently big, the change in SOC is relatively small. As a result, the transient charge and discharge processes can be simplified as a steady-state process.
(2) An isothermal condition is assumed in the entire domain.
(3) The membrane is impermeable to all ions and species, except for protons.
(4) Possible side reactions, such as hydrogen and oxygen evolutions, are not considered.

2.2. Governing equations

2.2.1. Transport through the porous electrode

To model the mass transport in the porous electrode, we express the molar flux of each species, $\vec{N}_i$ (with i representing $V^{2+}, V^{3+}, VO^{2+}, VO_2^+, H^+, HSO_4^-$), in terms of the modified Nernst–Planck equation as:

$$\vec{N}_i = -D_i^{eff}\nabla c_i - Fz_i c_i \xi_i \nabla \phi_l + \vec{u} c_i \quad (5)$$

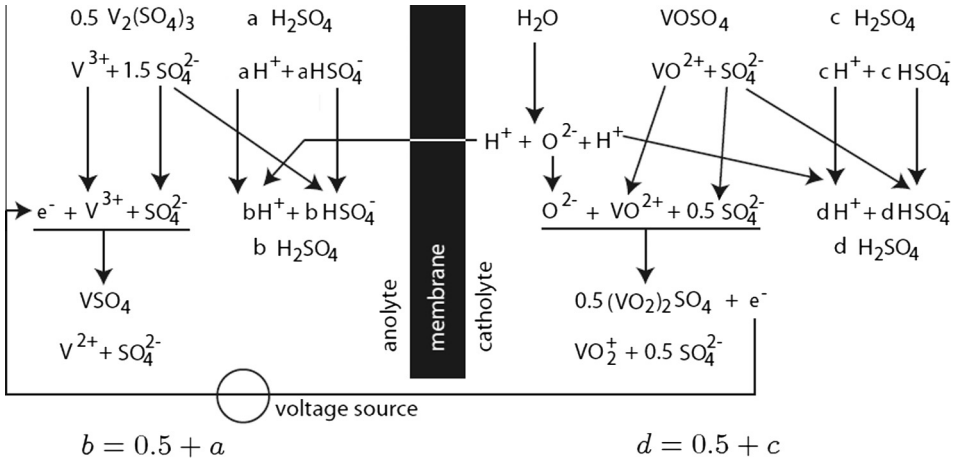

Fig. 1. Illustration of the anolyte and catholyte component variations from SOC = 0 to SOC = 1.

Table 1
Geometric and operating parameters.

Parameters	Symbols	Value	Unit	Reference
Specific surface area	A_r	2×10^5	m^{-1}	[29]
Electrode thickness	δ_e	3×10^{-3}	m	
Polymer electrolyte membrane	δ_{mem}	1.8×10^{-4}	m	
Electrode height	h	2×10^{-2}	m	
Electrode width	w	2×10^{-2}	m	
Operating temperature	T	300	K	
Electrode porosity	ε_0	0.7	1	
Electrode fiber diameter	d_f	17.6	μm	[29]
Initial V^{2+} ion concentration	$c^0_{V(II)}$	1050	mol m^{-3}	
Initial V^{3+} ion concentration	$c^0_{V(III)}$	450	mol m^{-3}	
Initial VO^{2+} ion concentration	$c^0_{V(IV)}$	450	mol m^{-3}	
Initial VO_2^+ ion concentration	$c^0_{V(V)}$	1050	mol m^{-3}	
HSO_4^- ion concentration	$c^0_{HSO_4^-}$	2000	mol m^{-3}	
Initial H^+ ion concentration	$c^0_{H^+}$	2000	mol m^{-3}	
Current density	I	400	A m^{-2}	
Electrolyte volumetric flow rate	Q	0.3	ml s^{-1}	
Pump efficiency	ψ_{pump}	0.9	1	

where c_i represents the concentration of each species, F is the Faradaic constant, z_i and ξ_i are the valence and ionic mobility of each species, ϕ_l is the ionic potential in the electrolyte, and

$$D_i^{eff} = D_i \varepsilon^{1.1}(1 + 1.46 \times 10^{-3}\mathrm{Pe}^2) \tag{6}$$

is the effective diffusion coefficient of each species which includes the effect of flow dispersion, with ε and D_i representing, respectively, the porosity of the electrode and the free-space diffusivity of each species [24]. The superficial electrolyte velocity $\vec{u}$ can be expressed using Darcy's law as:

$$\rho \frac{v}{K}\vec{u} = -\nabla p \tag{7}$$

where K is the permeability of the porous electrode, v is the kinematic viscosity of the electrolyte and p is the liquid pressure. The liquid pressure is determined from an overall mass balance as:

$$\nabla \cdot \vec{u} = 0 \tag{8}$$

The flow of charged species gives the current in electrolyte solution:

$$\vec{i}_i = z_i F \vec{N}_i \tag{9}$$

The electrolyte is considered to be electrically neutral:

$$\sum_i z_i c_i = 0 \tag{10}$$

Combining Eqs. 5, 9 and 10, we can express the total current density in the electrolyte as:

$$\vec{i} = \sum_i \vec{i}_i = -F\sum_i z_i D_i^{eff} \nabla c_i - F^2 \sum_i z_i^2 c_i \xi_i \nabla \phi_l \tag{11}$$

The conservation of species can be written as:

$$\nabla \cdot \vec{N}_i = \dot{R}_i \tag{12}$$

where $\dot{R}_i$ is the generation rate for species i [17].

Combining Eqs. (5) and (12) gives:

$$\nabla \cdot (\vec{u} c_i) = \nabla \cdot \left(D_i^{eff} \nabla c_i\right) + \nabla \cdot (F z_i c_i \xi_i \nabla \phi_l) + \dot{R}_i \tag{13}$$

Due to the conservation of charge, the charge entering the electrolyte solution is balanced by the charge leaving the solid phase:

$$\nabla \cdot \vec{i} = \nabla \cdot \vec{i}_l = -\nabla \cdot \vec{i}_s \tag{14}$$

where $\vec{i}_l$ is the current density in the electrolyte solution and $\vec{i}_s$ is the current density in the solid matrix.

The electronic potential in the solid matrix is given by Ohm's law:

$$-\sigma_s^{eff} \nabla^2 \phi_s = \nabla \cdot \vec{i}_s \tag{15}$$

where σ_s^{eff} and ϕ_s are the effective conductivity and electronic potential of the solid matrix.

2.2.2. Transport through the membrane

As proton is the only mobile ion, the current conservation equation is:

$$\vec{N}_{H^+} = -\frac{\sigma_{mem}}{F} \nabla \phi_{mem} \tag{16}$$

where σ_{mem} and ϕ_{mem} are the conductivity and electric potential of the ion-exchange membrane. The values of the constants related to mass and charge transport can be found in Table 2. It is worth noting that the constant value of electrolyte viscosity used for comparison represents the electrolyte viscosity of negative half-cell at the SOC of 1.0.

2.2.3. Reaction kinetics

The electrochemical reactions taking place at the solid surfaces of the porous graphite electrode can be expressed using the Butler–Volmer Equation as [22]:

$$j_1 = \varepsilon A_v F k_1 \left(c^s_{V(III)}\right)^{\alpha_{-,1}} \left(c^s_{V(II)}\right)^{\alpha_{+,1}} \left\{\exp\left(\frac{\alpha_{+,1} F \eta_1}{RT}\right) - \exp\left(-\frac{\alpha_{-,1} F \eta_1}{RT}\right)\right\} \tag{17}$$

and

$$j_2 = \varepsilon A_v F k_2 \left(c^s_{V(V)}\right)^{\alpha_{-,2}} \left(c^s_{V(IV)}\right)^{\alpha_{+,2}} \left\{\exp\left(\frac{\alpha_{+,2} F \eta_2}{RT}\right) - \exp\left(-\frac{\alpha_{-,2} F \eta_2}{RT}\right)\right\} \tag{18}$$

Eqs. (17) and (18) are for the negative and positive electrodes, respectively, where A_v is specific surface area of the porous electrode, k_1 and k_2 are the standard rate constants for negative and positive electrochemical reactions, $c_i^s, i \in \left\{V^{2+}, V^{3+}, VO^{2+}, VO_2^+\right\}$ are the vanadium-species concentrations at the liquid–solid interfaces of the porous region, α_+ and α_- are the anodic and cathodic transfer coefficients, η_1 and η_2 are the overpotentials in the negative and positive electrodes, respectively. The electrochemical constants and coefficients are listed in Table 3.

The interface concentrations c_i^s can be related to the bulk concentrations c_i by balancing the electrochemical reaction rate with the rate of mass transfer of the reactants to (or from) the electrode surface. For the negative electrode during discharge, the balance is:

Table 2
Transport properties.

Parameters	Symbols	Value	Unit	Reference
V^{2+} ion diffusivity in electrolyte	$D_{V(II)}$	2.4×10^{-10}	$m^2\ s^{-1}$	[30]
V^{3+} ion diffusivity in electrolyte	$D_{V(III)}$	2.4×10^{-10}	$m^2\ s^{-1}$	[30]
VO^{2+} ion diffusivity in electrolyte	$D_{V(IV)}$	3.9×10^{-10}	$m^2\ s^{-1}$	[30]
VO_2^+ ion diffusivity in electrolyte	$D_{V(V)}$	3.9×10^{-10}	$m^2\ s^{-1}$	[30]
Water diffusivity in membrane	$D_{H_2O}^{eff}$	5.75×10^{-10}	$m^2\ s^{-1}$	[17]
Proton diffusivity in membrane	$D_{H^+}^{eff}$	3.5×10^{-10}	$m^2\ s^{-1}$	[31]
HSO_4^- ion diffusivity in membrane	$D_{HSO_4^-}^{eff}$	2.2×10^{-10}	$m^2\ s^{-1}$	[17]
Carman-Kozeny constant	K_{CK}	5.55		[17]
Constant electrolyte kinematic viscosity	ν	1.2×10^{-6}	$m^2\ s^{-1}$	
Electrolyte density	ρ	1400	$kg\ m^{-3}$	
Conductivity of the solid phase	σ_m	1000	$S\ m^{-1}$	
Conductivity of the membrane	σ_{mem}	10	$S\ m^{-1}$	

Table 3
Electrochemistry properties.

Parameters	Symbols	Value	Unit	Reference
Cathodic transfer coefficient for reaction (1)	$\alpha_{-,1}$	0.5		Assumed
Anodic transfer coefficient for reaction (1)	$\alpha_{+,1}$	0.5		Assumed
Cathodic transfer coefficient for reaction (2)	$\alpha_{-,2}$	0.5		Assumed
Anodic transfer coefficient for reaction (2)	$\alpha_{+,2}$	0.5		Assumed
Standard rate constant for reaction (1)	k_1	1.75×10^{-7}	$m\ s^{-1}$	[17]
Standard rate constant for reaction (2)	k_2	3.0×10^{-9}	$m\ s^{-1}$	[31]
Equilibrium potential for reaction (1)	E_1^0	−0.26	V	[22]
Equilibrium potential for reaction (2)	E_2^0	1.004	V	[22]

$$k_m\left(c_{V(II)} - c^s_{V(II)}\right) = \varepsilon k_1\left[c^s_{V(II)}\exp\left(\frac{\alpha_{+,1}F\eta_1}{RT}\right) - c^s_{V(III)}\exp\left(-\frac{\alpha_{-,1}F\eta_1}{RT}\right)\right] \quad (19)$$

and

$$k_m\left(c_{V(III)} - c^s_{V(III)}\right) = \varepsilon k_1\left[c^s_{V(III)}\exp\left(\frac{\alpha_{-,1}F\eta_1}{RT}\right) - c^s_{V(II)}\exp\left(-\frac{\alpha_{+,1}F\eta_1}{RT}\right)\right] \quad (20)$$

where k_m is the mass transfer coefficient and can be expressed as [24]:

$$k_m = D_i(2 + 1.534Re^{0.912})/d_p \quad (21)$$

Combining Eqs. (19) and (20), we can express the concentrations of *V(II)* and *V(III)* ions at the liquid–solid interface as:

$$c^s_{V(II)} = \frac{k_m c_{V(II)} + \varepsilon k_1 k_m c_{V(III)}\exp\left(-\frac{\alpha_{-,1}F\eta_1}{RT}\right)/A_1}{B_1 - C_1/A_1} \quad (22)$$

and

$$c^s_{V(III)} = \frac{k_m c_{V(III)} + \varepsilon k_1 k_m c_{V(II)}\exp\left(-\frac{\alpha_{+,1}F\eta_1}{RT}\right)/B_1}{A_1 - C_1/B_1} \quad (23)$$

where

$$A_1 = k_m + \varepsilon k_1\exp\left(\frac{\alpha_{-,1}F\eta_1}{RT}\right) \quad (24)$$

$$B_1 = k_m + \varepsilon k_1\exp\left(\frac{\alpha_{+,1}F\eta_1}{RT}\right) \quad (25)$$

and

$$C_1 = (\varepsilon k_1)^2\exp\left(\frac{-\alpha_{+,1} - \alpha_{-,1}}{RT}F\eta_1\right) \quad (26)$$

A similar approach can be used to solve the concentrations of *V(IV)* and *V(V)* at the liquid–solid interface of positive electrode.

The overpotentials in Eqs. (17) and (18) are defined as:

$$\eta_1 = \phi_{m,1} - \phi_{s,1} - E_1 \quad (27)$$

and

$$\eta_2 = \phi_{m,2} - \phi_{s,2} - E_2 \quad (28)$$

where E_1 and E_2 are thermodynamic equilibrium potentials for reactions (1) and (2), respectively, and can be approximated using the relevant Nernst equation as:

$$E_1 = E_1^0 + \frac{RT}{F}\ln\frac{c_{V(III)}}{c_{V(II)}} \quad (29)$$

and

$$E_2 = E_2^0 + \frac{RT}{F}\ln\frac{c_{V(V)}c^2_{H^+}}{c_{V(IV)}} \quad (30)$$

where the equilibrium potentials E_1^0 and E_2^0 are given in Table 3. Then the cell voltage can be written as:

$$E_{cell} = E_2^0 - E_1^0 + \frac{RT}{F}\ln\frac{c_{V(V)}c_{V(II)}c^2_{H^+}}{c_{V(IV)}c_{V(III)}} - |\eta_1| - |\eta_2| - IR_{cell}\ \text{(discharge)} \quad (31)$$

and

$$E_{cell} = E_2^0 - E_1^0 - \frac{RT}{F}\ln\frac{c_{V(V)}c_{V(II)}c^2_{H^+}}{c_{V(IV)}c_{V(III)}} + |\eta_1| + |\eta_2| + IR_{cell}\ \text{(charge)} \quad (32)$$

where I is the current density and R_{cell} is the cell electrical resistance.

2.3. Boundary conditions

The boundary conditions can be specified by referring to Fig. 2 as follows:

At $x = 0$,

$$\frac{\partial\phi_{s,1}}{\partial x} = 0, \quad \phi_{m,1} = 0 \quad (33)$$

$$\frac{\partial p}{\partial x} = 0, \quad \frac{\partial p}{\partial y} = 0 \quad (34)$$

$$\frac{\partial c_i}{\partial x} = 0, \quad i = V^{2+}, V^{3+}, H^+, HSO_4^- \quad (35)$$

At $x = x_1$,

$$\phi_{s,1} = \phi_{mem} \tag{36}$$

$$\vec{N}_i \cdot \vec{n} = 0, \quad i = V^{2+}, V^{3+}, HSO_4^- \tag{37}$$

$$\vec{i}_s \cdot \vec{n} = \vec{i}_{mem} \cdot \vec{n} \text{ (for proton)} \tag{38}$$

At $x = x_2$, the interfacial conditions are similar to those at $x = x_1$,

$$\phi_{s,2} = \phi_{mem} \tag{39}$$

$$\vec{N}_i \cdot \vec{n} = 0, \quad i = VO^{2+}, VO_2^+, HSO_4^- \tag{40}$$

$$\vec{i}_{mem} \cdot \vec{n} = \vec{i}_s \cdot \vec{n} \text{ (for proton)} \tag{41}$$

At $x = x_3$,

$$\frac{\partial \phi_{s,2}}{\partial x} = 0, \quad -\sigma_m^{eff} \frac{\partial \phi_{m,2}}{\partial x} = I \tag{42}$$

$$\frac{\partial p}{\partial x} = 0, \quad \frac{\partial p}{\partial y} = 0 \tag{43}$$

$$\frac{\partial c_i}{\partial x} = 0, \quad i = VO^{2+}, VO_2^+, H^+, HSO_4^- \tag{44}$$

At $y = 0$,

$$\frac{\partial \phi_s}{\partial y} = 0, \quad \frac{\partial \phi_m}{\partial y} = 0 \tag{45}$$

$$c_i = c_i^0, \quad i = V^{2+}, V^{3+}, H^+ \text{ and } HSO_4^- \text{ when } 0 < x < x_1$$

$$i = VO^{2+}, VO_2^+, H^+ \text{ and } HSO_4^- \text{ when } x_2 < x < x_3 \tag{46}$$

$$\vec{u} \cdot \vec{n} = u_{in} \tag{47}$$

where

$$c_i^0 = c_{total} \cdot SOC\left(\text{for } V^{2+} \text{ and } VO_2^+\right) \tag{48}$$

$$c_i^0 = c_{total} \cdot (1 - SOC)(\text{for } V^{3+} \text{ and } VO^{2+}) \tag{49}$$

At $y = h$,

$$\frac{\partial \phi_s}{\partial y} = 0, \quad \frac{\partial \phi_m}{\partial y} = 0 \tag{50}$$

$\frac{\partial c_i}{\partial y} = 0$, $i = V^{2+}$, V^{3+}, H^+ and HSO_4^- when $0 < x < x_1$;

$$i = VO^{2+}, VO_2^+, H^+ \text{ and } HSO_4^- \text{ when } x_2 < x < x_3 \tag{51}$$

$$p = p_{out} \tag{52}$$

At all the boundaries except the inlet/outlet, the pressure satisfies the Neumann condition:

$$\nabla p \cdot \vec{n} = 0 (\text{except inlet/outlet}) \tag{53}$$

The interfacial boundary conditions (Eqs. (38) and (41)) are based on the current balance to associate the variables in both electrodes for iterative solution.

3. The correlations of the SOC-dependent viscosity of anolyte and catholyte

To consider the effect of the SOC-dependent viscosity of both anolyte and catholyte, the correlations of the respective electrolyte viscosity in terms of SOC are required. In this work, the correlations are obtained through a theoretical analysis. The basic idea for predicting the electrolyte viscosity is to utilize the viscosities of binary solutions (i-H_2O) which compose the VRFB electrolyte. From Eyring's absolute rate theory, for an electrolyte solution the viscosity can be expressed as [25]:

$$v_{mix} = v_{id} \exp\left(\frac{\Delta G^{\neq}}{RT}\right) \tag{54}$$

with

$$v_{id} = \exp\left(\sum_i x_i \ln v_i^{pure}\right) \tag{55}$$

where v_{mix} and v_{id} are the kinematic viscosities of a mixed solution and an ideal solution, respectively. Superscript *pure* together with subscript i represent the property of pure substance. $\Delta G^{\neq}$ is the molar excess activation free energy,

$$\Delta G^{\neq} = \beta RT \sum z_i x_i \ln a_i \tag{56}$$

where β is a system-specific constant for non-ideal solutions, z_i,a_i and x_i are the stoichiometric coefficient, the activity and molar fraction of the component.

If an electrolyte is made up of n electrolyte solutes and one solvent (generally water), Eq. (54) can be rewritten as:

$$\ln v_{mix} = \sum_i x_i \ln v_i^{pure} + x_{H_2O} \ln v_{H_2O}^{pure} + \frac{1}{RT} \Delta G^{\neq} \tag{57}$$

with

$$x_i = m_i \Big/ \left((1000/M_{H_2O}) + \sum_{i=1}^{n} m_i\right) \tag{58}$$

where m_i is the molality (mol/kg).

Similarly, for a binary solution, the viscosity can be expressed as:

$$\ln v_i^{(i,0)} = x_i^{(i,0)} \ln v_i^{pure} + x_{H_2O}^{(i,0)} \ln v_{H_2O}^{pure} + \frac{1}{RT} \Delta G_i^{\neq(i,0)} \tag{59}$$

where the variables with the superscript (i,0) together with the subscript i to denote the quantities of i in the binary solution (i-H_2O) having the same water activity as that of the mixed solution.

Combining Eqs. (56) and (59), the viscosity of the electrolyte can be expressed as:

$$\ln v_{mix} = \sum_i \frac{x_i}{x_i^{(i,0)}} \ln v_i^{(i,0)} + \beta \sum_i z_i x_i \ln\left(\frac{z_i m_i}{\sum_i z_i m_i}\right) \tag{60}$$

or

$$\ln \mu_{mix} = \sum_i \frac{x_i}{x_i^{(i,0)}} \ln \mu_i^{(i,0)} + \beta \sum_i z_i x_i \ln\left(\frac{z_i m_i}{\sum_i z_i m_i}\right) + \left(\ln \rho_{mix} - \sum_i \frac{x_i}{x_i^{(i,0)}} \ln \rho_i^{(i,0)}\right) \tag{61}$$

where ρ is the density. It is worth noting that in a dilute solution system, the last two terms in the right-hand side of Eq. (61) can be eliminated (Note the value of $\rho_i^{(i,0)}$ is close to that of ρ_{mix} and $\sum_i \frac{x_i}{x_i^{(i,0)}} = 1$) as an approximation. Based on the experimental data in [15] and the data we measured with a viscometer (Brookfield®), the relationships between the dynamic viscosity (Pa·s) and concentration (mol/L) for VSO_4, $V_2(SO_4)_3$, $VOSO_4$ and $(VO_2)_2SO_4$ solutions (with water as solvent) can be fitted as follows:

$$\mu_{b,V(II)} = \left(1.362 + 0.251 c_{V(II)} + 0.15 c_{V(II)}^2\right)/1000 \tag{62}$$

$$\mu_{b,V(III)} = \left(1.913 - 0.855 c_{V(III)} + 1.05 c_{V(III)}^2\right)/1000 \tag{63}$$

$$\mu_{b,V(IV)} = \left(2.751 + 1.61 c_{V(IV)} + 2.05 c_{V(IV)}^2\right)/1000 \tag{64}$$

and

$$\mu_{b,V(V)} = \left(2.875 - 0.45 c_{V(V)} + 1.5 c_{V(V)}^2\right)/1000 \tag{65}$$

where $\mu_{b,i}$ is the dynamic viscosity of i in the binary solution (i-H_2O).

According to Eq. (61), we can obtain the expressions for the viscosities of anolyte and catholyte in a VRFB:

$$\ln \mu_1 = \frac{x_{V(II)}}{x^{(i,0)}_{V(II)}} \cdot \ln((1.362 + 0.215 \times c_{V,total} \times SOC + 0.15 \times (c_{V,total} \times SOC)^2)/1000) + \frac{x_{V(III)}}{x^{(i,0)}_{V(III)}} \cdot \ln((1.913 - 0.855 \times c_{V,total} \times (1 - SOC) + 1.05 \times (c_{V,total} \times (1 - SOC))^2)/1000) + \frac{x_{H_2SO_4}}{x^{(i,0)}_{H_2SO_4}} \cdot \ln((0.941 + 0.144 \times (c_{H_2SO_4} + c_{V,total} \times 0.5 \times SOC) + 0.025 \times (c_{H_2SO_4} + c_{V,total} \times 0.5 \times SOC)^2)/1000) + \frac{x_{H_2O}}{x^{(i,0)}_{H_2O}} \cdot \ln \mu_{H_2O} \quad (66)$$

$$\ln \mu_2 = \frac{x_{V(V)}}{x^{(i,0)}_{V(V)}} \cdot \ln((2.875 - 0.45 \times c_{V,total} \times SOC + 1.51 \times (c_{V,total} \times SOC)^2)/1000) + \frac{x_{V(IV)}}{x^{(i,0)}_{V(IV)}} \cdot \ln((2.751 + 1.61 \times c_{V,total} \times (1 - SOC) + 2.05 \times (c_{V,total} \times (1 - SOC))^2)/1000) + \frac{x_{H_2SO_4}}{x^{(i,0)}_{H_2SO_4}} \cdot \ln((0.941 + 0.144 \times (c_{H_2SO_4} + c_{V,total} \times 0.5 \times SOC) + 0.025 \times (c_{H_2SO_4} + c_{V,total} \times 0.5 \times SOC)^2)/1000) + \frac{x_{H_2O}}{x^{(i,0)}_{H_2O}} \cdot \ln \mu_{H_2O} \quad (67)$$

To validate Eqs. (66) and (67), we consider a VRFB electrolyte consisting of 1.5 M $VOSO_4$ and 3.0 M H_2SO_4 (SOC = 0) as reported elsewhere [13]. The dynamic viscosity according to Eq. (67) is 1.69 mPa·s which is close to the experimental data of 1.97 mPa·s. We also measured the catholyte viscosities at SOC = 0.5 (1.58 mPa·s) and SOC = 1 (1.47 mPa·s). The calculated values from Eq. (67) are 1.43 and 1.34 mPa·s respectively. For the anolyte, the measured values at SOC = 0 and SOC = 1 are 1.85 and 1.36 mPa·s and the calculated values from Eq. (66) are 1.66 and 1.23 mPa·s respectively. The comparison indicates that the equations can accurately predict the electrolyte viscosity.

Eqs. (66) and (67) are plotted in Fig. 3 (The electrolytes consist of 1.5 M vanadium ions and 2.0 M H_2SO_4). The equations are integrated into the numerical model.

4. Results and discussion

The variables in the conservation equations were iteratively solved using the self-written code based on the finite-volume method. The relative error tolerance was set to 1.0E−6.

4.1. Model validation

The numerical solutions are validated against the experimental data in the literature [26]. Since the cell voltages were measured as a function of time, the time-dependant experimental data need to be transformed to the SOC-dependant data for the purpose of comparison. The transformation is made according to [19]:

$$SOC = SOC^0 + \frac{t}{t_0}(SOC^e - SOC^0) \quad (68)$$

where t_0 is the total charge (or discharge) time, SOC^0 and SOC^e represent, respectively, the value of SOC at the beginning and end of the discharge (or charge). The comparison between the numerical and experimental data is shown in Fig. 4. It can be seen that the model captures the trend well. The small discrepancies in the cell voltage between the numerical results and the experimental data at high SOCs may be caused by the presence of side reactions, which are not accounted in the present model. In addition, the cell performance predicted by the present model is compared with that predicted from the model with a constant electrolyte viscosity. Under the same operating conditions, the cell voltage solved from the latter is lower during the charge process and higher during the discharge process. Hence, ignoring the variation of electrolyte viscosity will overestimate the cell performance in the whole range of SOC.

4.2. Pressure drop

Fig. 5 shows the pressure drop distributions in the positive and negative electrodes at SOC = 0.7. As can be seen, the pressure drop through the positive electrode reaches as high as 2978 Pa while that in the negative side is 2676 Pa. The difference is induced by the divergence in viscosity, as the viscosity of the positive electrolyte is higher than that of the negative electrolyte. By comparison, applying the commonly used assumption that the electrolyte viscosity is a constant (1.2mPa·s) the pressure drop in either the

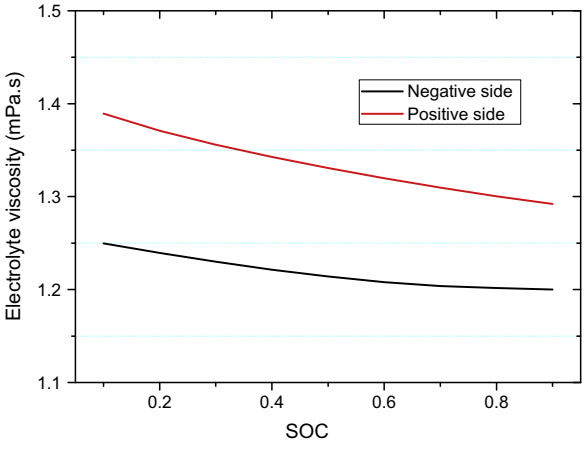

Fig. 3. Variations in the electrolyte viscosity with SOC in the positive and negative half-cells.

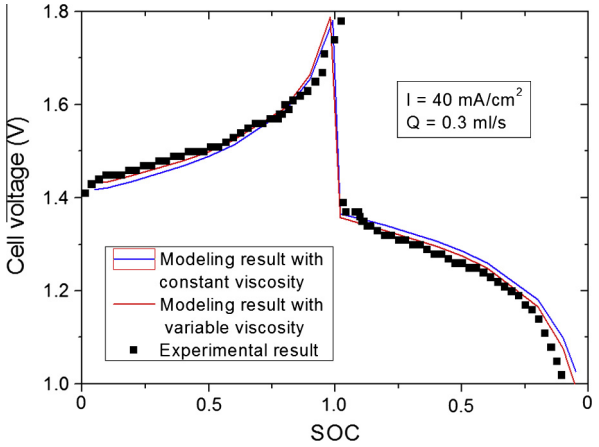

Fig. 4. Cell performance comparison between numerical solutions and experimental data.

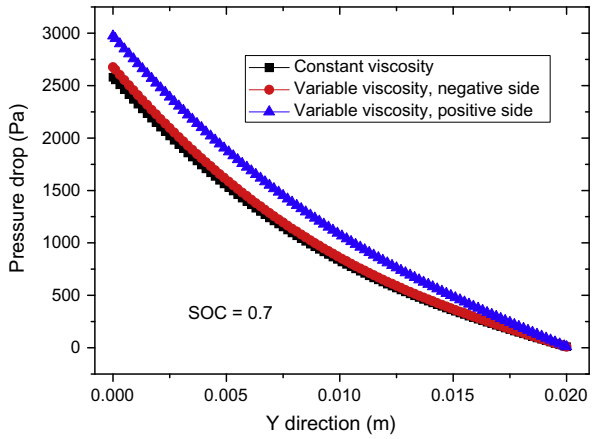

Fig. 5. Pressure drops across the electrode resulting from the present model and the constant-viscosity model.

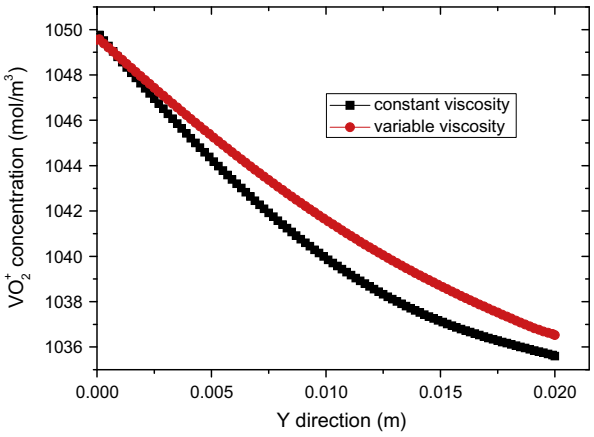

Fig. 7. Distributions of the VO_2^+ concentration resulting from the present model and the constant-viscosity model.

positive or the negative side is 2590 Pa. Moreover, the velocities in the positive and negative electrodes can be obtained. Fig. 6 shows the distributions of the velocity at the middle of the positive electrode. It can be seen that a larger viscosity causes sharper velocity profile, but the difference is rather small. The velocity distribution is used to solve other variables such as the ions concentrations, electrode overpotential and local current density.

4.3. Distributions of concentration, overpotential and local current density

The distributions of VO_2^+ concentration at the middle line of the positive electrode at the discharge current density of 40 mA/cm^2 are presented in Fig. 7 (at SOC = 0.7). During discharge, VO_2^+ is consumed along the flow direction such that the concentration decreases from the inlet to the outlet. At any position within the electrode, the VO_2^+ concentration resulting from the present model is higher than that from the constant-viscosity model. This difference is caused by the difference in the velocity distribution inside the porous electrode.

Fig. 8 shows the overpotential distributions obtained through two models in the cross-section of $y = 0.01$ m under the discharge current density of 40 mA/cm^2. It is worth mentioning that according to the definition given by Eq. (28), the overpotential of the positive electrode is less than zero during discharge. For convenience, here we show the absolute value of the overpotential. As can be seen, the overpotential rises from the region near the membrane

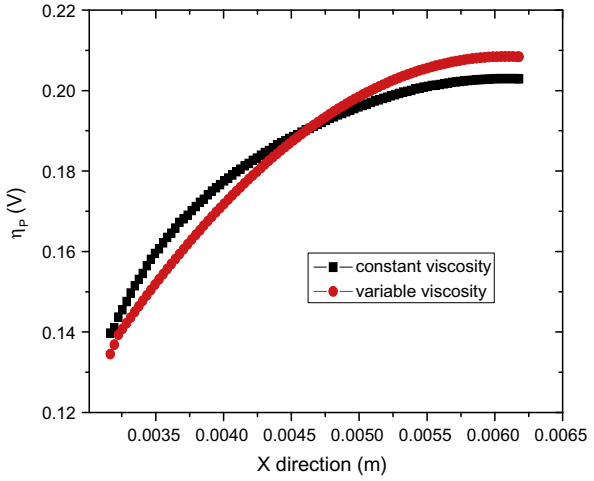

Fig. 8. Distributions of the overpotential in the positive electrode resulting from the present model and the constant-viscosity model.

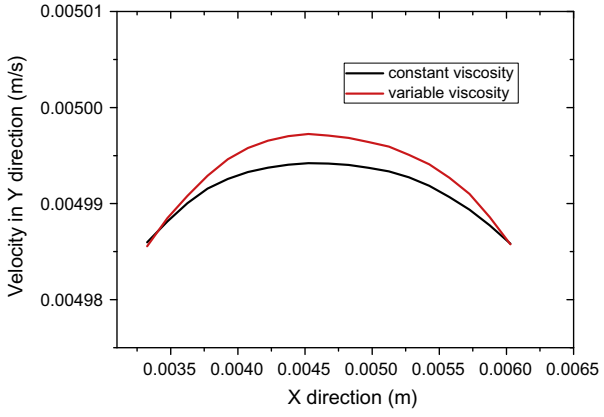

Fig. 6. Distributions of the velocity at the middle of the postive electrode.

to the region close to the current collector in order to maintain the current. The difference in the overpotential along the electrolyte flow direction is extremely small, since the concentration difference from the inlet to the outlet is small. The overpotential distribution resulting from the present model is steeper than that from the constant-viscosity model. In detail, the overpotential obtained through the present model is higher in the region near the membrane, whereas in the region close to the current collector, the distribution of overpotential is reverse. At the interface of current collector and positive electrode ($x = 0.00618$ m), the absolute value of overpotential obtained through the present model is 0.209 V, while the value is 0.20 V when applying a constant-viscosity model.

The distribution of the local current density in the cross-section of $y = 0.01$ m is shown in Fig. 9. The local current density changes remarkably in the electrode thickness direction. Less current is generated in the region near the membrane and the maximum current density occurs in the region close to the current collector. The current density resulting from the present model is steeper than that from the constant-viscosity model. The reason leading to this divergence can be explained as follows. The electrochemical reaction rate is determined by both the local overpotential and local reactant concentrations. As the concentration difference is rather small (see Fig. 7), the quantity of local current density is primarily

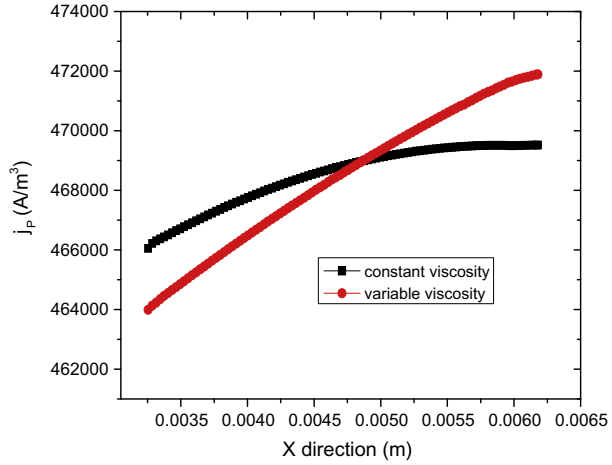

Fig. 9. Distributions of the local current density resulting from the present model and the constant-viscosity model.

affected by the local overpotential distribution. As shown in Fig. 8, the overpotential obtained from the present model distributes more steeply than does that from the constant-viscosity model, causing the corresponding distribution of current density.

4.4. System efficiency

Under practical operating conditions, the pumps continuously circulate the electrolyte between tanks and cell, consuming a part of energy in the VRFB system, which lowers the system efficiency. Including this effect, the energy-based system efficiency can be defined as [27,28]:

$$\psi_{energy} = \frac{W_{disch} - W_{pump,disch}}{W_{char} + W_{pump,char}} \tag{69}$$

where W_{disch} is the VRFB output work during discharge and W_{char} is the input work during the charge process. The pumping works can be expressed as:

$$W_{pump,disch} = Qt_{disch}\Delta p/\psi_{pump} \tag{70}$$

and

$$W_{pump,char} = Qt_{char}\Delta p/\psi_{pump} \tag{71}$$

where Q is the flow rate, ψ_{pump} is the pump efficiency and Δp is the pressure drop through the battery.

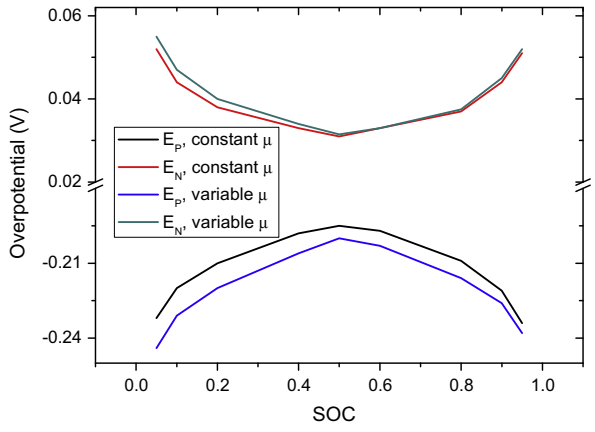

Fig. 10. Variations in the overpotential with SOC.

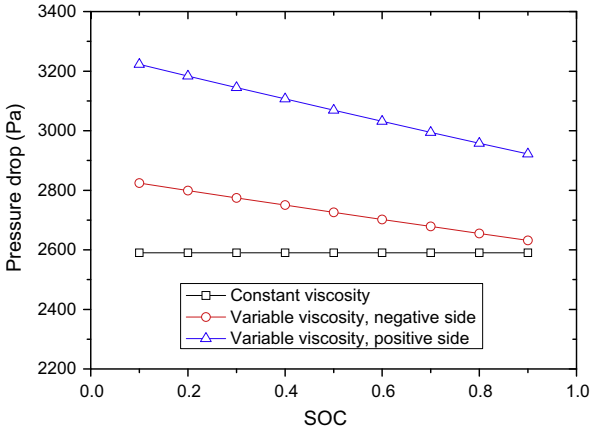

Fig. 11. Variations in the pressure drop with SOC.

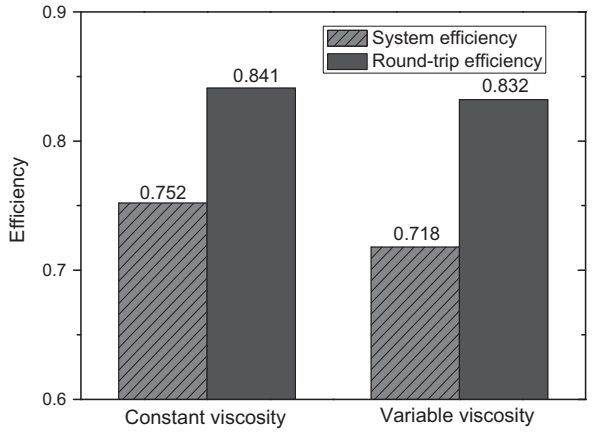

Fig. 12. Energy-based efficiency and the round-trip efficiency resulting from the present model and the constant-viscosity model.

To solve W_{disch} and W_{char}, the cell voltages in the whole range of SOC is needed. Fig. 10 shows the variation in the positive and negative half-cell overpotentials in the VRFB obtained through the present model and the constant-viscosity model, respectively. Since the local electrochemical reaction rate is related with the concentrations of two species (See Eqs. (17)), the minimum value of overpotential appears around SOC of 0.5, while the maximum value is at the lowest or highest SOC. The discrepancy in overpotentials resulting from two models is larger in positive half-cell, where the sluggish kinetics results in a larger overpotential. After obtaining the values of overpotential, the corresponding cell voltages can be solved, as already shown in Fig. 4. At all SOCs, the cell voltage obtained through the present model is higher during the charge process and is lower during the discharge process. However, the difference is less than 20 mV.

In order to obtain the values of W_{pump}, the pressure drops at various SOCs are solved and shown in Fig. 11. Both the pressure drops for the negative and positive sides keep constant in the full range of SOC for the constant-viscosity model. In contrast, for the case of variable viscosity, the pressure drops keep decreasing as the SOC rises. Moreover, at each SOC the pressure drop is larger in the positive half-cell since the electrolyte viscosity in positive side is larger than that in negative side.

With the solved pumping work and battery work for a charge–discharge cycle, the energy-based system efficiencies obtained through the present model and the constant- electrolyte-viscosity

model are shown in Fig. 12. The efficiency is 0.752 for the former and is 0.718 for the latter. For comparison, the round-trip efficiencies (*RTE*, the ratio of the energy output during discharge to the energy input during charge process within a charge–discharge cycle) for the two cases are also illustrated. For the former, *RTE* is 0.841; for the latter it becomes 0.832. The results show that the system efficiency including the pumping energy loss can reflect the energy generation and consumption in a VRFB more veritably, since the pumping energy is not neglectable in practical operations. Moreover, the difference between the energy-based system efficiency and *RTE* for that resulting from the present model is larger than that from the constant- viscosity model, implying that the previous studies have underestimated the effect of electrolyte viscosity in VRFBs.

5. Conclusions

In this work, a 2-D mass-transport and electrochemical model for a VRFB is developed, which takes the effect of SOC-dependent electrolyte viscosity into account. The model is used to investigate the distributions of vanadium ions concentration, overpotential and local current density of a single vanadium redox cell. Compared with the results resulting from a constant-electrolyte-viscosity model, the results from this model exhibit higher pressure drop (especially in the positive half-cell), steeper distributions of overpotential and local current density in the electrodes. The comparison of modeling results indicates that the consideration of the SOC-dependent electrolyte viscosity enables a more realistic simulation and more accurate estimations of pumping work and the system efficiency of VRFBs.

Acknowledgement

The work described in this paper was fully supported by a grant from the Research Grants Council of the Hong Kong Special Administrative Region, China (Project No. 623313).

References

[1] Sum E, Rychcik M, Skyllas-Kazacos M. Investigation of the V(V)/V(IV) system for use in the positive half-cell of a redox battery. J Power Sour 1985;16:85–95.
[2] Skyllas-kazacos M, Rychcik M, Robins RG, Fane AG, Green MA. New all-vanadium redox flow cell. J Electrochem Soc 1986;133:1057–8.
[3] Skyllas-kazacos M, Grossmith F. J Electrochem Soc 1987;134:2950–3.
[4] Sum E, Skyllas-Kazacos M. A study of the V(II)/V(III) redox couple for redox flow cell applications. J Power Sour 1985;15:179–90.
[5] de Leon CP, Ferrer AF, Garcia JG, Szanto DA, Walsh FC. Redox flow cells for energy conversion. J Power Sour 2006;160:716–32.
[6] Huang KL, Li XG, Liu SQ, Tan N, Chen LQ. Research progress of vanadium redox flow battery for energy storage in China. Renew Energy 2008;33:186–92.
[7] Yang ZG, Zhang JL, Kintner MC. Electrochemical energy storage for green grid. Chem Rev 2011;111:3577–613.
[8] Li LY, Kim S, Wang W, Vijaayakumar M, Nie Z, Chen B. A stable vanadium redox-flow battery with high energy density for large-scale energy storage. Adv Energy Mater 2011;1:394–400.
[9] Tang C, Zhou DB. Methanesulfonic acid solution as supporting electrolyte for vanadium redox battery. Electrochim Acta 2012;65:179–84.
[10] Hu YF, Lee H. Prediction of viscosity of mixed electrolyte solutions based on the Eyring's absolute rate theory and the semi-ideal hydration model. Electrochim Acta 2003;48:1789–96.
[11] Wang PM, Anderko A, Young RD. Modeling viscosity of concentrated and mixed-solvent electrolyte systems. Fluid Phase Equilibria 2004;226:71–82.
[12] Mousa A. Chemical and electrochemical studies of V(III) and V(II) solutions in sulfuric acid solution for vanadium battery applications. PhD thesis, UNSW, Australia; 2003.
[13] Wen Y, Zhang H, Qian P, Zhao P, Zhou H, Yi BL. Investigation on the electrode process of concentrated V(IV)/V(V) species in a vanadium redox flow battery. Acta Phys-Chim Sinica 2006;22:403–8.
[14] Kausar N. Studies of V(IV) and V(V) species in vanadium cell electrolyte. PhD thesis, UNSW, Australia; 2002.
[15] Blanc C. Modeling of a Vanadium Redox Flow Battery Electricity Storage System. PhD thesis, Ecole Polytechnique Federal Lausanne, Switzerland; 2009.
[16] Kim S, Vijayakumar M, Wang W, Zhang J, Chen B, Li LY. Chloride supporting electrolytes for all-vanadium redox flow batteries. Phys Chem Chem Phys 2011;13:18186–93.
[17] Shah AA, Watt-Smith MJ, Walsh FC. A dynamic performance model for redox-flow batteries involving soluble species. Electrochim Acta 2008;53:8087–100.
[18] Fetlawi HA, Shah AA, Walsh FC. Non-isothermal modelling of the all-vanadium redox flow battery. Electrochim Acta 2009;55:78–89.
[19] You DJ, Zhang HM, Chen J. A simple model for the vanadium redox battery. Electrochim Acta 2009;54:6827–36.
[20] Shah AA, Fetlawi HA, Walsh FC. Dynamic modelling of hydrogen evolution effects in the all-vanadium redox flow battery. Electrochim Acta 2010;55:1125–39.
[21] Fetlawi HA, Shah AA, Walsh FC. Modelling the effects of oxygen evolution in the all-vanadium redox flow battery. Electrochim Acta 2010;55:3192–205.
[22] Vynnycky M. Analysis of a model for the operation of a vanadium redox battery. Energy 2011;36:2242–56.
[23] Knehr KW, Agar E, Dennison CR, Kalidindi AR, Kumbur EC. A transient vanadium flow battery model incorporating vanadium crossover and water transport through the membrane. J Electrochem Soc 2012;159:A1446–59.
[24] Xu Q, Zhao TS. Determinations of mass transport properties of vanadium ions through porous electrode of vanadium redox flow batteries. Phys Chem Chem Phys 2013;15:10841–8.
[25] Hu YF. Prediction of viscosity of mixed electrolyte solutions based on the Eyring's absolute rate theory and equations of Patwardham and Kumar. Chem Eng Sci 2004;59:2457–64.
[26] Qian P, Zhang HM, Chen J. A novel electrode-bipolar plate assembly for vanadium redox flow battery applications. J Power Sour 2008;175:613–20.
[27] Xu Q, Zhao TS, Leung PK. Numerical investigations of flow field designs for vanadium redox flow batteries. Appl Energy 2013;105:47–56.
[28] Blanc C, Rufer A. Optimization of the operating point of a vanadium redox flow battery. IEEE energy conversion congress and exposition 2009:2600–5.
[29] Zhou HT, Zhang HM, Zhao P, Yi BL. A comparative study of carbon felt and activated carbon based electrodes for sodium polysulfide/bromine redox flow battery. Electrochim Acta 2006;51:6304–12.
[30] Yamamura T, Watanabe M, Yano T, Shiokawa Y. Electron-transfer kinetics of Np^{3+}/Np^{4+}, NpO^{2+}/NpO_2^{2+}, V^{2+}/V^{3+}, and VO^{2+}/VO_2^{+} at carbon electrodes. J Electrochem Soc 2005;152:A830–6.
[31] Gattrell M, Park J, MacDougall B, Apte J, McCarthy S, Wu CW. Study of the mechanism of the V(IV)/V(V) redox reaction in acidic solutions. J Electrochem Soc 2004;151:A123–30.